Suppression of the charge ordered state in $Pr_{0.75}Na_{0.25}MnO_3$ at high pressure

2004 J. Phys.: Condens. Matter 16 5883

(http://iopscience.iop.org/0953-8984/16/32/021)

INSTITUTE OF PHYSICS PUBLISHING JOURNAL OF PHYSICS: CONDENSED MATTER

J. Phys.: Condens. Matter **16** (2004) 5883–5895 PII: S0953-8984(04)79960-9

Suppression of the charge ordered state in $Pr_{0.75}Na_{0.25}MnO_3$ at high pressure

D P Kozlenko[1,2], Z Jirák[3], I N Goncharenko[4] and B N Savenko[2]

[1] ISIS Facility, Rutherford Appleton Laboratory, Chilton, Didcot, Oxon OX11 0QX, UK
[2] Frank Laboratory of Neutron Physics, Joint Institute for Nuclear Research, 141980 Dubna Moscow Region, Russia
[3] Institute of Physics, Cukrovarnická 10, 162 53 Prague 6, Czech Republic
[4] Laboratoire Léon Brillouin, CEA-CNRS, CE Saclay, 91191 Gif-sur-Yvette Cedex, France

Received 27 April 2004
Published 30 July 2004
Online at stacks.iop.org/JPhysCM/16/5883
doi:10.1088/0953-8984/16/32/021

Abstract

The crystal and magnetic structures of the manganite $Pr_{0.75}Na_{0.25}MnO_3$ with non-integer mean valence (Mn^{3+}/Mn^{4+}) have been studied by means of powder neutron diffraction at high pressures up to 8 GPa in the temperature range 1.5–295 K. At ambient pressure, the system undergoes a charge ordering at $T_{CO} = 220$ K, followed by an onset of the AFM arrangement of the pseudo-CE (charge-exchange) type at $T_N = 170$ K. Under high external pressures, a suppression of the pseudo-CE-type AFM state and the concurrent appearance of the A-type AFM state are observed. The unconventional orientation of manganese magnetic moments in the A-type AFM phase inclined out of the [0 1 0] crystallographic plane indicates the presence of magnetic coupling between the A-type AFM regions, presumably of nanoscopic thickness, and the pseudo-CE-type AFM residual regions.

1. Introduction

The perovskite-type manganites $Ln_{1-x}A_xMnO_3$ (Ln—lanthanum or rare earth, A—alkaline earth elements) with non-integer Mn^{3+}/Mn^{4+} valence attract considerable interest in relation to the close interrelation of the magnetic and electronic properties [1]. The rich spectrum of magnetic ground states observed in these compounds is a result of a competition between ferromagnetic (FM) interactions mediated by itinerant charge carriers (the double-exchange mechanism [2–4]) and antiferromagnetic superexchange interactions between localized spins of manganese ions, which are combined with lattice and orbital degrees of freedom [5]. The balance can be effectively tuned via the choice of trivalent Ln and divalent A elements in the perovskite A-sites and their ratio.

In special cases the charge carriers can be trapped by a self-induced local distortion, giving rise to various charge and orbitally ordered configurations. Typical examples are

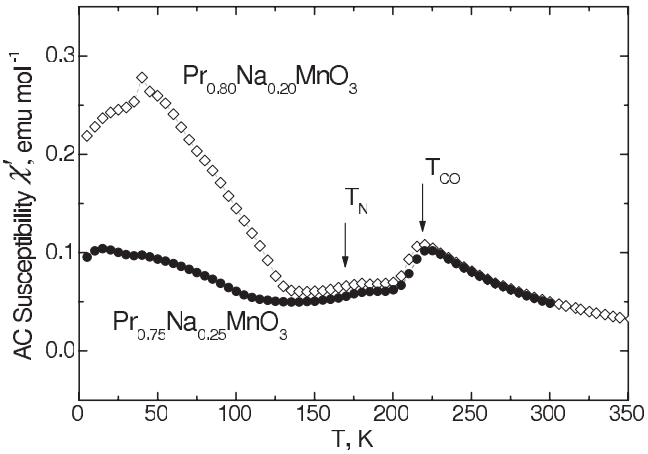

Figure 1. Temperature dependences of the real component of the AC susceptibility observed for samples $Pr_{1-x}Na_xMnO_3$ ($x = 0.2$ and 0.25). The arrows mark the charge ordering temperature and a weak anomaly at the AFM transition. The susceptibility increase below 120 K is associated with the formation of fluctuating FM clusters.

furnished by manganites in the half-doped range, i.e. close to the ratio of $Mn^{3+}/Mn^{4+} = 0.50{:}0.50$, which exhibit an antiferromagnetic (AFM) ground state of the CE (charge-exchange) type, as found for $La_{0.5}Ca_{0.5}MnO_3$ [6], $Pr_{0.5}Ca_{0.5}MnO_3$ [7], $Nd_{0.5}Ca_{0.5}MnO_3$ [8] and $Nd_{0.5}Sr_{0.5}MnO_3$ [9]. Of interest are the charge ordered systems with a shifted Mn^{3+}/Mn^{4+} ratio that exhibit a pseudo-CE AFM arrangement, in particular the compounds $Pr_{1-x}Ca_xMnO_3$ with $x = 0.3$–0.4 [7, 10]. In the pseudo-CE-type AFM state there are two magnetic sublattices formed by ordered Mn^{3+} and Mn^{4+} ions which correspond to propagation vectors $q_1 = (0\ 0\ 1/2)$ and $q_2 = (1/2\ 0\ 1/2)$, respectively [1, 7, 10]. The application of external magnetic fields [11, 12] or light illumination [13, 14] destroys the charge ordered state of these systems and leads to the appearance of the FM metallic state. Alternatively, application of high external pressure or tuning of the average A-site ionic radius [15] leads to the destabilization of the charge ordered state and the appearance of the A-type (layered) AFM state with metallic conductivity in the FM layers. A pressure-induced phase transition to the A-type AFM state with collective carriers was observed in the pseudo-CE system $Pr_{0.7}Ca_{0.3}MnO_3$ [16] and assumed to occur in CE-type $Nd_{0.5}Sr_{0.5}MnO_3$ on the basis of resistivity data [17]. The effect was interpreted in terms of the one-electron bandwidth which becomes broader with increasing overlap of manganese and oxygen orbitals and acquires a quasi-two-dimensional character due to anisotropic lattice compression under high pressure [16].

Recently, the charge ordered insulating state was evidenced in less common manganites doped with monovalent alkaline ions—$Pr_{1-x}Na_xMnO_3$ ($Pr_{1-x}Na_x[(Mn^{3+})_{1-2x}(Mn^{4+})_{2x}]O_3$) with $x \sim 0.2$–0.25, which exhibit colossal magnetoresistance effects in medium magnetic fields [12]. At ambient conditions these manganites are paramagnetic insulators with an orthorhombic structure (space group $Pnma$) and undergo a charge ordering below $T_{CO} \sim 220$ K followed by an onset of the pseudo-CE-type AFM state below $T_N \sim 170$ K. In addition to the majority pseudo-CE phase, ferromagnetic (FM) clusters are formed which are responsible for the spin-glass character of the real component of the AC susceptibility versus temperature data measured at the frequency 900 Hz (figure 1) [12]. The total amount of charge disordered spin-glass regions in the sample $x = 0.2$ can be estimated to be at most 10%. The

estimation is based on the measured value of the linear term in the low temperature specific heat. The formation of the FM clusters is largely suppressed in the sample with $x = 0.25$ (figure 1).

It was assumed that the charge ordered insulating and ferromagnetic metallic states in $Pr_{1-x}Na_xMnO_3$ ($x = 0.2, 0.25$) are nearly degenerate and may be reversed by diverse means, including application of external pressure [12]. Later structural study of the sample $Pr_{0.8}Na_{0.2}MnO_3$ with an actual Mn^{3+}/Mn^{4+} ratio 0.65:0.35 showed, however, that at high external pressure $P \sim 3$ GPa a microscopically separated state is formed, consisting of a mixture of the majority A-type AFM phase regions and only minor FM phase regions which are probably metastable [18]. The observed pressure-induced changes of the magnetic state were ascribed to the decisive role of anisotropic compression of the lattice.

Much less formation of FM clusters in $Pr_{0.75}Na_{0.25}MnO_3$ indicates that the degeneracy of the charge ordered pseudo-CE and FM states is less pronounced in this compound in comparison with $Pr_{0.8}Na_{0.2}MnO_3$. The present paper is focused on pressure effects on the crystal and magnetic structure of $Pr_{0.75}Na_{0.25}MnO_3$ with an actual Mn^{3+}/Mn^{4+} ratio of 0.61:0.39 and describes powder neutron diffraction experiments at high pressures up to 8 GPa over the temperature range 1.5–290 K.

2. Experimental details

The compound of nominal composition $Pr_{0.75}Na_{0.25}MnO_3$ was prepared by a solid state reaction, as described in detail in [12]. The electron microprobe analysis of perovskite grains showed, however, that the real Pr/Na ratio was shifted to about 0.80:0.20 due to sodium loss and liquid phase formation upon sintering. Consistently, the wet chemical analysis determined the actual ratio of Mn^{3+}/Mn^{4+} (0.61:0.39) instead of the expected one (0.50:0.50).

The crystal structure of $Pr_{0.75}Na_{0.25}MnO_3$ was investigated using the Pearl/HiPr diffractometer at the ISIS pulsed neutron spallation source (Rutherford Appleton Laboratory, UK). The Paris–Edinburgh high pressure cell [19] was used with a 4:1 volume mixture of fully deuterated methanol–ethanol as a pressure transmitting medium. A TiZr encapsulated gasket of 90 mm^3 initial volume was used to attain nearly hydrostatic compression of the sample in the pressure range studied [20]. For the pressure determination, an equation of state (pressure dependence of the unit cell volume) of $Pr_{0.75}Na_{0.25}MnO_3$ was measured using a ∼2:1 volume mixture of the sample with NaCl as a reference material [21]. Diffraction patterns were collected by a detector bank covering the scattering angle range $83° < 2\theta < 97°$. The experiments were performed in the pressure range 0–8 GPa and temperature range 100–295 K. Typical data collection times were about 3–6 h. The diffraction data were analysed by the Rietveld method using the general structure analysis system (GSAS) [22].

The magnetic structure of $Pr_{0.75}Na_{0.25}MnO_3$ was investigated with the G6.1 diffractometer at the Orphée reactor (Laboratoire Léon Brillouin, France). The incident neutron wavelength was 4.74 Å. The sample with a volume about 1 mm^3 was loaded in the sapphire anvil high pressure cell [23]. Several tiny ruby chips were placed at different points of the sample surface and the pressure was determined by a standard ruby fluorescence technique. Measurements of the pressure distribution on the sample yield typical pressure inhomogeneities of ±5%. Neutron focusing systems [24] and special cadmium protection were used to increase the neutron flux at the sample position and achieve a low background level, respectively. The measurements were performed in the pressure range 0–6.5 GPa and temperature range 1.5–295 K. Typical data collection times were about 5–7 h. The diffraction data were analysed by the Rietveld method using the FULLPROF program [25].

Table 1. Structural parameters of $Pr_{0.75}Na_{0.25}MnO_3$ at selected pressures and temperatures. The atomic positions are: Mn 4(b) (0, 0, 0.5), Pr/Na and O1 4(c) (x, 1/4, z) and O2 8(d) (x, y, z) of the space group *Pnma*. Values of Mn–O1 and Mn–O2 bond lengths and Mn–O1–Mn and Mn–O2–Mn bond angles are also presented.

P (GPa)	0	2.7	2.7	5.2	7.9	8.3
T (K)	295	295	100	295	100	295
a (Å)	5.432(1)	5.402(1)	5.406(1)	5.375(1)	5.352(1)	5.344(1)
b (Å)	7.680(2)	7.645(2)	7.637(3)	7.60(2)	7.556(2)	7.532(2)
c (Å)	5.451(1)	5.421(5)	5.428(2)	5.402(1)	5.391(2)	5.383(5)
Pr/Na: x	0.019(2)	0.015(3)	0.023(2)	0.018(2)	0.003(4)	0.008(3)
z	−0.003(4)	0.002(5)	−0.006(5)	0.004(4)	−0.009(4)	0.010(6)
O1: x	0.492(2)	0.500(3)	0.503(3)	0.497(3)	0.494(3)	0.488(3)
z	0.060(2)	0.065(2)	0.066(2)	0.065(2)	0.067(2)	0.066(2)
O2: x	0.285(1)	0.281(1)	0.281(1)	0.279(1)	0.276(1)	0.272(1)
y	0.036(1)	0.034(1)	0.032(1)	0.033(1)	0.034(1)	0.033(1)
z	0718(1)	0.722(1)	0.719(1)	0.723(1)	0.724(1)	0.728(1)
Mn–O1 (Å)	1.948(8)	1.944(6)	1.943(5)	1.932(5)	1.923(5)	1.917(5)
Mn–$O2_a$ (Å)	1.971(8)	1.955(7)	1.944(7)	1.943(7)	1.925(6)	1.919(7)
Mn–$O2_b$ (Å)	1.949(8)	1.934(7)	1.946(7)	1.925(7)	1.927(6)	1.921(7)
Mn–O1–Mn	160.5(6)°	159.1(6)°	158.6(6)°	159.1(6)°	158.3(6)	158.3(6)°
Mn–O2–Mn	157.9(5)°	159.6(5)°	160.0(5)°	160.2(5)°	160.8(5)	161.2(5)°
R_p (%)	6.47	5.97	3.84	5.46	2.97	3.91
R_{wp} (%)	4.13	3.86	4.26	3.72	3.29	3.58

3. Results

3.1. Crystal structure at high pressure

Neutron diffraction patterns of $Pr_{0.75}Na_{0.25}MnO_3$ measured at different pressures and ambient temperature at the Pearl/HiPr diffractometer are shown in figure 2. Over the whole pressure (0–8 GPa) and temperature (100–295 K) range studied $Pr_{0.75}Na_{0.25}MnO_3$ retains the initial orthorhombic structure of *Pnma* symmetry with the unit cell four times enlarged with respect to the simple perovskite subcell, $a \approx c \approx a_p\sqrt{2}$ and $b \approx 2a_p$. The structural parameters obtained from the Rietveld refinement of the diffraction data at high pressures are presented in table 1. The values of the lattice parameters at ambient pressure agree well with ones obtained in [12].

The pressure dependence of the unit cell volume obtained for $Pr_{0.75}Na_{0.25}MnO_3$ at room temperature is shown in figure 3. The compressibility data were fitted with the third-order Birch–Murnaghan equation of state [26]:

$$P = \tfrac{3}{2}B_0(x^{-7/3} - x^{-5/3})[1 + \tfrac{3}{4}(B' - 4)(x^{-2/3} - 1)],$$

where $x = V/V_0$ is the relative volume change, V_0 is the unit cell volume at $P = 0$ and B_0, B' are the bulk modulus ($B_0 = -V(\mathrm{d}P/\mathrm{d}V)_T$) and its pressure derivative ($B' = (\mathrm{d}B_0/\mathrm{d}P)_T$). The calculated values $B_0 = 157(5)$ GPa and $B' = 4(1)$ are comparable with those determined in [27], $B_0 = 178$ GPa and $B' = 4$, for the manganite $La_{0.75}Ca_{0.25}MnO_3$ with a similar orthorhombic structure.

The pressure dependence of the lattice parameters is also shown in figure 3. The linear compressibilities $k_i = -(1/a_{i0})(\mathrm{d}a_i/\mathrm{d}P)_T$ ($a_i = a, b, c$) along the a and b axes, $k_a = 0.0021(2)$ GPa^{-1} and $k_b = 0.0022(2)$ GPa^{-1}, are slightly larger than that along the c axis, $k_c = 0.0016(2)$ GPa^{-1}. These values are close to those reported for $La_{0.75}Ca_{0.25}MnO_3$ [27] and $Pr_{0.8}Na_{0.2}MnO_3$ [18].

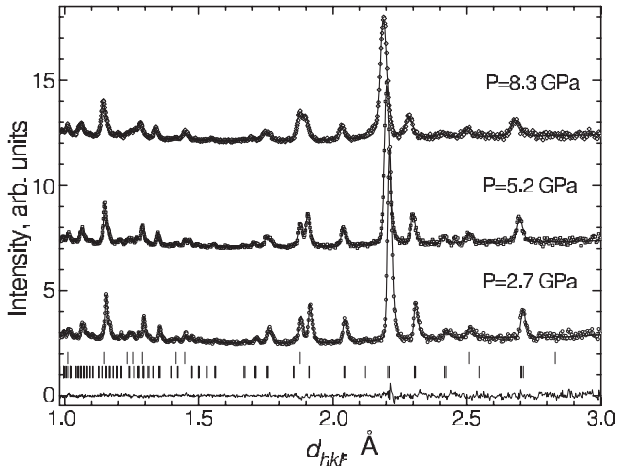

Figure 2. Parts of the neutron diffraction patterns of $Pr_{0.75}Na_{0.25}MnO_3$, measured at the Pearl/HiPr diffractometer at $P = 2.7$, 5.2 and 8.3 GPa and ambient temperature and processed by the Rietveld method. Experimental points, calculated profiles and the difference curve (for $P = 2.7$ GPa, bottom) are shown. The ticks below represent calculated positions of diffraction peaks of $Pr_{0.75}Na_{0.25}MnO_3$ (lower row) and tungsten carbide (WC) coming from the anvils of the high pressure cell (upper row) whose contribution was also included in calculations.

In the orthorhombic structure of $Pr_{0.75}Na_{0.25}MnO_3$ the MnO_6 octahedra consist of one pair of Mn–O1 bonds oriented along the crystallographic b axis and two pairs of Mn–O2 bonds lying within the (ac) plane. At ambient conditions, one pair of Mn–O2 bond lengths is longer than the other pair of Mn–O2 and the pair of Mn–O1 bond lengths, which have close values (table 1). As a result, apically elongated MnO_6 octahedra with a pseudo-tetragonal distortion $t_p = 2l_{Mn-O2a}/(l_{Mn-O2b} + l_{Mn-O1}) = 1.011(2)$ alternate regularly along the [101] and [10$\bar{1}$] directions, as is characteristic for the O′ perovskite phase. The value of t_p is close to that found for $Pr_{0.7}Ca_{0.3}MnO_3$, which also exhibits the pseudo-CE AFM state at low temperatures, $t_p = 1.010$ [28]. Upon the application of pressure, the Mn–O1 and Mn–O2 bond lengths decrease nearly linearly, although with different slopes (figure 4). As a result, the MnO_6 octahedra become more symmetrical under high pressure with the result that, at $P = 8.3$ GPa, all Mn–O bond lengths have nearly equal lengths $l_{Mn-O} \approx 1.92$ Å and $t_p = 1.000(2)$. The average ⟨Mn–O–Mn⟩ bond angle increases with pressure from 158.8° at $P = 0$ to 160.2° at $P = 8.3$ GPa (figure 5). The data in table 1 at $T = 100$ K refer to the *Pnma* space group and neglect thus the eventual $2a \times b \times c$ superstructure in charge ordered $Pr_{0.75}Na_{0.25}MnO_3$. In spite of such a limitation, the results show that the application of high pressure $P = 2.7$ GPa at 100 K leads to some decrease of the Mn–O1 bond in comparison with the average of the Mn–O2 bonds. This results in a small compression of MnO_6 octahedra along the [0 1 0] direction with a corresponding pseudo-tetragonal distortion $t_p = l_{Mn-O1}/\langle l_{Mn-O2}\rangle = 0.999(2)$. At higher pressure $P = 7.9$ GPa and $T = 100$ K a similar temperature-induced deformation of MnO_6 octahedra was observed, with $t_p = 0.998(2)$. The average ⟨Mn–O–Mn⟩ bond angle changes only slightly with temperature decrease under high pressure and its variation does not exceed the experimental accuracy.

3.2. Magnetic structure at high pressure

Neutron diffraction patterns of $Pr_{0.75}Na_{0.25}MnO_3$ obtained at ambient pressure and temperatures 200, 50 and 1.5 K at the G6.1 diffractometer are shown in figure 6. On cooling

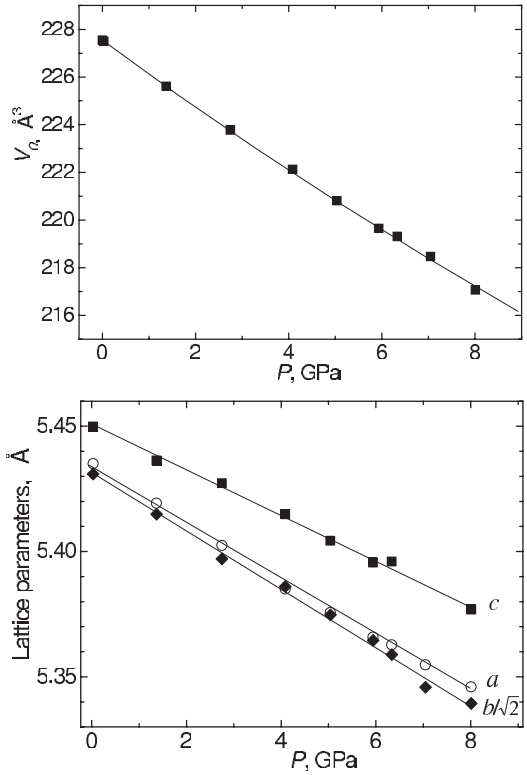

Figure 3. The pressure dependence of the unit cell volume of $Pr_{0.75}Na_{0.25}MnO_3$ fitted by the third-order Birch–Murnaghan equation of state and lattice parameters fitted by linear functions (solid lines). The error bars are within the symbol sizes.

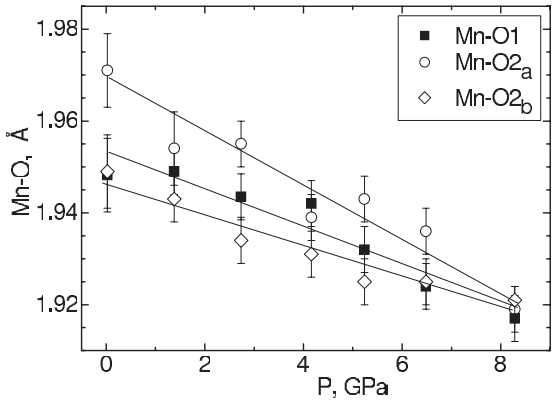

Figure 4. Mn–O1 and Mn–O2 bond lengths of $Pr_{0.75}Na_{0.25}MnO_3$ as functions of pressure at ambient temperature. Solid lines represent linear fits to the experimental data.

to $T < T_N = 170$ K, the appearance of single and overlapping magnetic peaks (0 0 1/2), (1/2 0 1/2), (1 0 1/2), (0 0 3/2)/(0 2 1/2) and (1/2 0 3/2)/(3/2 0 1/2)/(1/2 2 1/2) was observed. This corresponds to the onset of the pseudo-CE-type AFM state with two magnetic sublattices formed by ordered Mn^{3+} and Mn^{4+} ions with propagation vectors $q_1 = (0\ 0\ 1/2)$

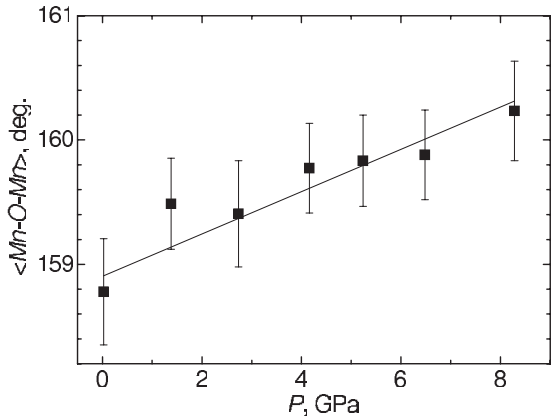

Figure 5. The average ⟨Mn–O–Mn⟩ bond angle of $Pr_{0.75}Na_{0.25}MnO_3$ as a function of pressure at ambient temperature. The solid line represents a linear fit to the experimental data.

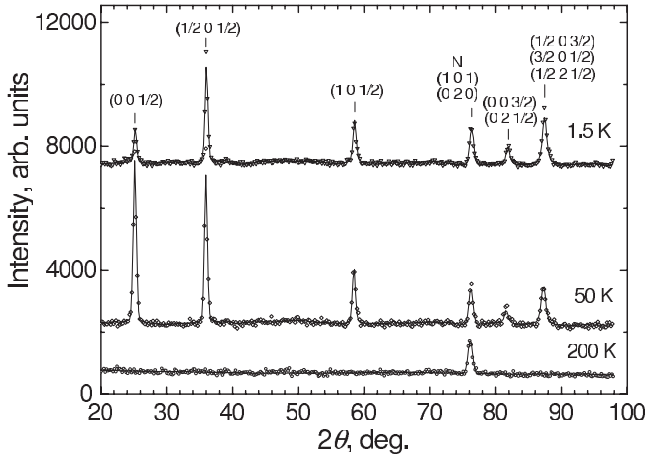

Figure 6. Parts of neutron diffraction patterns for $Pr_{0.75}Na_{0.25}MnO_3$, measured at the G6.1 diffractometer at ambient pressure and $T = 200$, 50 and 1.5 K and processed by the Rietveld method. Experimental points and calculated profiles are shown. Indices of magnetic peaks of pseudo-CE-type AFM structure and nuclear peaks are given. The nuclear peaks are labelled with the letter N.

and $q_2 = (1/2\ 0\ 1/2)$, respectively. The Mn magnetic moments are oriented along the b axis and their values, obtained from the Rietveld refinement of experimental data, are nearly the same for the two magnetic sublattices, $\mu_1 = 3.1(1)$ and $\mu_2 = 3.0(1)\ \mu_B$ at $T = 50$ K, and agree with those obtained for $Pr_{0.8}Na_{0.2}MnO_3$ in [12]. For $T < 50$ K a decrease of the $(0\ 0\ 1/2)$ and $(1/2\ 0\ 1/2)$ magnetic peak intensities was observed (figure 7). Such a behaviour is similar to that found for $Pr_{0.8}Na_{0.2}MnO_3$ in [12] and can be associated with the reorientation of the manganese magnetic moments. The analysis of the diffraction data obtained at $T = 1.5$ K shows that the pseudo-CE-type AFM coupling remains unchanged but the moments rotate from the [0 1 0] to the [0 0 1] axis by the angle $\varphi = 63°$. Their magnitudes are nearly the same as for $T = 50$ K, $\mu_1 \approx \mu_2 = 3.1(1)\ \mu_B$. No increase of the (101)/(020) nuclear peak intensity in the temperature range 1.5–295 K was observed, indicating the absence of the long range ordered FM component.

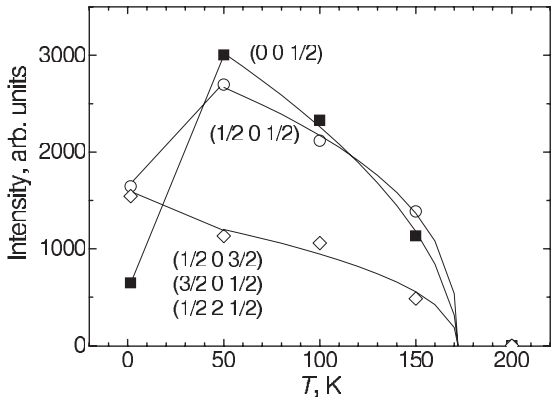

Figure 7. Temperature dependences of integrated intensities of AFM peaks (0 0 1/2), (1/2 0 1/2) and (1/2 0 3/2)/(3/2 0 1/2)/(1/2 2 1/2) for $Pr_{0.75}Na_{0.25}MnO_3$ at ambient pressure.

At $P = 2.6$ GPa, the appearance of magnetic peaks corresponding to the pseudo-CE-type AFM phase was also observed below $T_N \approx 170$ K (figure 8). However, in comparison with the ambient pressure data, their integrated intensities become much weaker than that of the nuclear peak (101)/(020) which varies only slightly with the pressure and temperature change. At $P = 2.6$ GPa and $T = 100$ K the values of intensity ratio $I(0\,0\,1/2)/I[(1\,0\,1)/(0\,2\,0)] = 0.37$ and $I(1/2\ 0\ 1/2)/I[(1\ 0\ 1)/(0\ 2\ 0)] = 0.41$ are significantly lower than those at ambient pressure, 3.05 and 2.77, respectively. Moreover, for $T < 170$ K an additional contribution to the intensity of the magnetic peaks (1/2 0 1/2) and (1/2 0 3/2)/(3/2 0 1/2)/(1/2 2 1/2) located at $2\theta \approx 36°$ and 86.5° was detected (figure 8). This cannot be explained in terms of the reorientation or canting of Mn magnetic moments of the pseudo-CE-type AFM structure and may be attributed to the appearance of a layered A-type AFM phase. In the A-type AFM structure Mn magnetic moments form ferromagnetic planes with an antiferromagnetic coupling between them. Its characteristic feature is the apical compression of MnO_6 octahedra along the direction perpendicular to the ferromagnetic planes [29–31]. Although the crystal structure data (table 1) reflect rather negligible apical compression of the MnO_6 octahedra at $T = 100$ K and high pressure, the shift of A-type magnetic peaks with decreasing temperature reveals at 1.5 K an increase of the average of the a,c lattice parameters by ∼0.2% and significant decrease of the b parameter by ∼1.2%. Such a lattice deformation is similar to that found for the A-type AFM phase of $Pr_{0.8}Na_{0.2}MnO_3$ [18] and $Pr_{0.7}Ca_{0.3}MnO_3$ [16] at high pressure, although about twice smaller in comparison with that for the A-type AFM phase of $Nd_{1-x}Sr_xMnO_3$ at ambient pressure [29]. One finds that the apical compression of the MnO_6 octahedra along the b axis increases in the A-type regions of $Pr_{0.75}Na_{0.25}MnO_3$ to about $t_p = 0.985(4)$. On the other hand, the regions of pseudo-CE-type AFM order exhibit smaller lattice deformation of ∼0.1–0.3%, similar to those found for $Pr_{0.8}Na_{0.2}MnO_3$ [12] and $Pr_{0.7}Ca_{0.3}MnO_3$ [28]. This difference results in a shift between positions of diffraction peaks corresponding to pseudo-CE-type and A-type AFM phases, which is obvious from figure 8. However, the average resolution of the diffractometer was not enough for us to fully resolve the peaks of these two phases.

From the above one may assume that in the A-type AFM phase of $Pr_{0.75}Na_{0.25}MnO_3$ the Mn magnetic moments form ferromagnetic planes perpendicular to the crystallographic [0 1 0] direction with the antiferromagnetic coupling between them. Thus, the corresponding propagation vector is $q = (0\ 1\ 0)$. The analysis of the diffraction data shows that at 50 K the manganese magnetic moments in the A-type AFM structure have components $\mu_{xz} = 0.6(1)\ \mu_B$

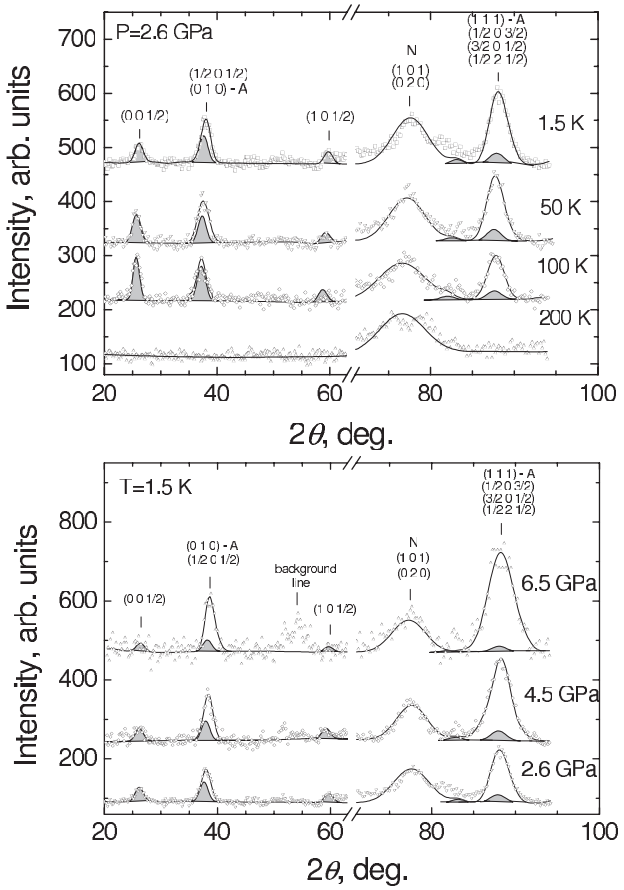

Figure 8. Parts of neutron diffraction patterns for $Pr_{0.75}Na_{0.25}MnO_3$, measured at the G6.1 diffractometer at different pressures and temperatures and processed by the Rietveld method. Experimental points and calculated profiles are shown. Indices of AFM peaks of pseudo-CE-type and A-type AFM magnetic structures as well as nuclear peaks are given. The magnetic peaks of the A-type AFM phase and nuclear peaks are labelled with the letters A and N, respectively.

lying in the FM planes and $\mu_y = 1.1(1)\ \mu_B$ oriented out-of-plane and are thus inclined at about 29° from the b axis. The moments increase as temperature decreases and pressure increases, as shown in table 2, while the inclination angle remains nearly unchanged.

The analysis of the pseudo-CE-type AFM diffraction peak intensities shows that the Mn magnetic moments reorient around 50 K from [0 1 0] towards the [0 0 1] direction, similar to what is observed at $P = 0$. The inclination angle from the b axis reaches the value $\varphi \approx 45°$–$50°$ at $T = 1.5$ K, irrespective of the high pressure value (see table 2).

Under high pressure, the Neél temperature corresponding to the onset of the pseudo-CE-type AFM state remains nearly the same, T_N(pseudo-CE) = 170(10) K, and the temperature corresponding to the onset of the A-type AFM state increases from $T_N(A) = 165(10)$ K at 2.6 GPa to 185(10) K at 6.5 GPa with $dT_N/dP \approx 5$ K GPa^{-1}. These values were obtained from the analysis of the temperature dependences of the integrated intensities of the magnetic peak (0 0 1/2) coming from the pseudo-CE-type AFM phase and the magnetic peak located at $2\theta \approx 86.5°$ which contains the majority contribution from the (1 1 1) peak of the

Table 2. Components of Mn magnetic moments in the pseudo-CE-type and A-type AFM phases of $Pr_{0.75}Na_{0.25}MnO_3$ at selected pressures and temperatures. Values of the angle φ between the magnetic moments and the b axis are also given.

P (GPa)		2.6			4.5			6.5	
T (K)	150	50	1.5	150	50	1.5	150	50	1.5
Pseudo-CE-type AFM phase									
$\mu_{y1} \approx \mu_{y2}$ (μ_B)	0.5(1)	0.8(1)	0.6(1)	0.7(1)	0.7(1)	0.5(1)	0.5(1)	0.7(1)	0.5(1)
$\mu_{z1} \approx \mu_{z2}$ (μ_B)	—	0.2(1)	0.6(1)	—	0.2(1)	0.6(1)	—	0.2	0.5(1)
φ_{CE} (deg)	0	14	45	0	16	50	0	16	45
A-type AFM phase									
μ_y (μ_B)	0.4(1)	1.1(1)	1.2(1)	0.9(1)	0.9(1)	1.1(1)	1.1(1)	1.8(1)	2.1(1)
μ_{xz} (μ_B)	0.2(1)	0.6(1)	0.6(1)	0.4(1)	0.6(1)	0.6(1)	0.6(1)	0.8(1)	1.0(0)
φ_A (deg)	27	29	27	24	34	29	29	24	26
R_p (%)	5.14	5.95	6.26	4.12	4.21	3.76	5.50	5.69	5.29
R_{wp} (%)	6.47	7.64	8.37	5.30	5.51	4.72	7.03	7.54	6.94

A-type AFM phase (figure 9). They were fitted by the functions $I(T) \sim (1 - T/T_N)^{2\beta}$ with $\beta = 0.25$–0.33 and also using the experimental temperature dependences of the Mn magnetic moments determined at ambient pressure for the pseudo-CE-type AFM state of $Pr_{0.8}Na_{0.2}MnO_3$ in [12] and for the A-type AFM state of $Pr_{0.5}Sr_{0.5}MnO_3$ in [31]. Although such an approach is a rather crude approximation since the fractions of two coexisting magnetic phases may vary with temperature and pressure, the two methods give nearly equal values of T_N within the accuracy of its determination.

4. Discussion

Suppression of the charge ordered pseudo-CE-type AFM state and the concurrent appearance of the A-type AFM state under high pressure were observed previously in $Pr_{0.8}Na_{0.2}MnO_3$ [18] and $Pr_{0.7}Ca_{0.3}MnO_3$ [16]. A similar pressure-induced transformation was also assumed to occur under high pressure in $Nd_{0.5}Sr_{0.5}MnO_3$ with a related CE-type AFM ground state on the basis of resistivity data [17]. As in the case of $Pr_{0.8}Na_{0.2}MnO_3$ [18] and $Pr_{0.7}Ca_{0.3}MnO_3$ [16], the stabilization of the A-type AFM state in $Pr_{0.75}Na_{0.25}MnO_3$ should be related to the anisotropy of the lattice compression which leads to pronounced pseudo-tetragonal apical contraction of MnO_6 octahedra under high pressure along the [0 1 0] crystallographic direction. As has been shown recently, both experimentally [32] and theoretically [33], magnetic properties of CMR manganites are very sensitive to the tetragonal distortion c_p/a_p of the simple perovskite subcell. According to [33], the tetragonal distortion with $c_p/a_p < 1$ leads to an enhanced population of $d(x^2 - y^2)$ orbitals and a decrease of the first-nearest-neighbour exchange integral J_1 in the direction of the tetragonal contraction, which creates favourable conditions for a stabilization of the A-type AFM state. The apical lattice contraction along the b axis in $Pr_{0.75}Na_{0.25}MnO_3$ at high pressure and low temperature is close to one characteristic for the A-type AFM state of $Pr_{0.8}Na_{0.2}MnO_3$ [18] and $Pr_{0.7}Ca_{0.3}MnO_3$ [16]. The enhanced polarization of the $d(x^2 - y^2)$ orbitals in the A-type AFM state permits electron transfer within ferromagnetic planes, leading to the metallic-like conductivity with a two-dimensional character as observed for most of the known manganites of close average A-site ionic radius and carrier concentration [5, 30]. One would expect the A-type AFM state of $Pr_{0.75}Na_{0.25}MnO_3$ to also be metallic.

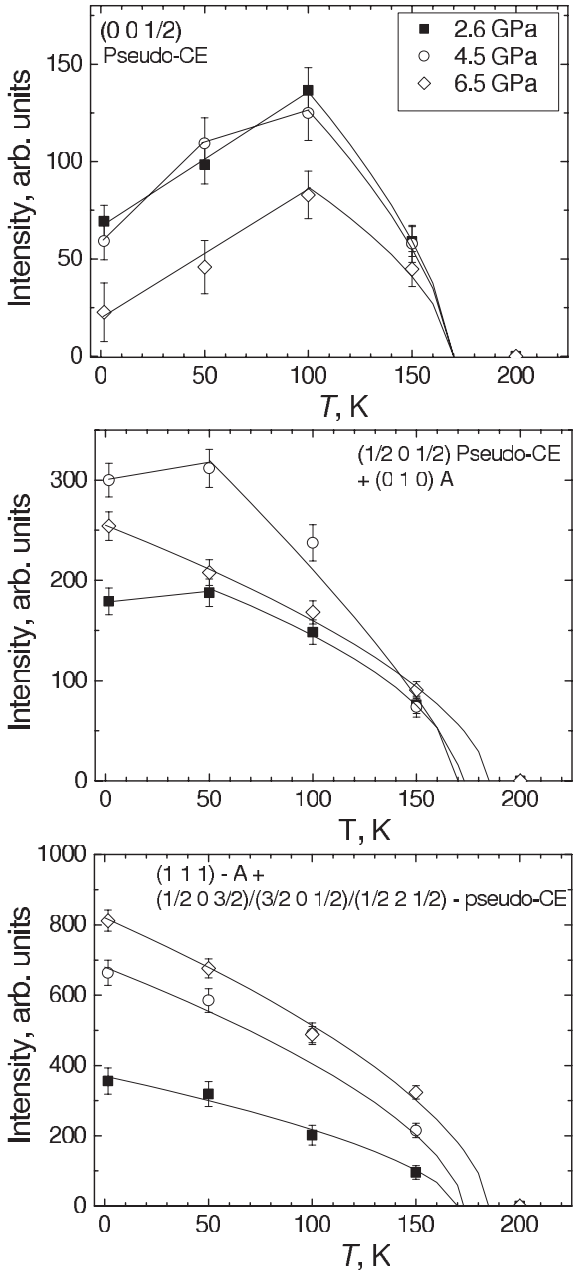

Figure 9. Temperature dependences of integrated intensities of selected AFM peaks of the pseudo-CE-type and A-type AFM phases in $Pr_{0.75}Na_{0.25}MnO_3$ at high pressure.

The orientation of Mn magnetic moments in the A-type AFM phase of $Pr_{0.75}Na_{0.25}MnO_3$ is different from the conventional A-type AFM order with Mn magnetic moments lying in the (ac) crystallographic planes, as found for $Pr_{0.8}Na_{0.2}MnO_3$ [18] and $Pr_{0.7}Ca_{0.3}MnO_3$ [16] at high pressure and also for $Pr_{1-x}Sr_xMnO_3$, $La_{1-x}Sr_xMnO_3$ [30, 31, 34] and $Nd_{1-x}Sr_xMnO_3$ [29] at ambient pressure (figure 10). The inclination of the Mn magnetic moments out of the (ac)

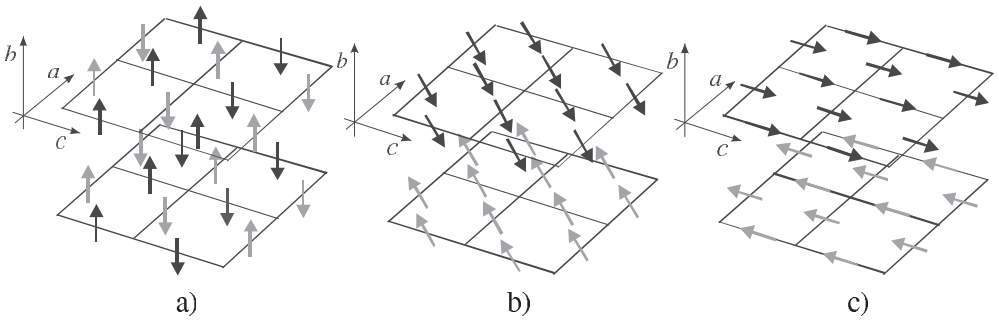

Figure 10. The pseudo-CE-type AFM structure of $Pr_{0.75}Na_{0.25}MnO_3$ at ambient pressure (a) and the proposed A-type AFM structure of $Pr_{0.75}Na_{0.25}MnO_3$ at high pressure (b). For comparison, the A-type AFM structure of $Pr_{0.8}Na_{0.2}MnO_3$ and $Pr_{0.7}Ca_{0.3}MnO_3$ at high pressure is also given (c).

planes in the A-type AFM phase of $Pr_{0.75}Na_{0.25}MnO_3$ may be attributed to the existence of magnetic exchange coupling between the A-type regions of presumably nanoscopic thickness and the residual regions of the pseudo-CE AFM phase which exhibit an easy magnetic axis along the *b* direction. An open question remains as to why the A-type spins do not reflect a reorientation in pseudo-CE phase below 50 K.

The neutron diffraction data on long range ordered moments given in table 2 suggest that the A-type AFM phase prevails at high pressures. The amount of the phase can, however, only be estimated. The fully ordered A-type AFM systems show generally Mn moment magnitudes of about $\mu = 3.0$–$3.5\ \mu_B$ while the averages for the present sample at 1.5 K are 1.3 and 2.3 μ_B for 2.6 and 6.5 GPa, respectively. This corresponds to a total volume of A-type ordered regions amounting to 20–50% of the sample. The remaining part contains the pseudo-CE regions and mainly disordered or short range ordered phase.

5. Conclusions

In summary, the results of our study show that application of high external pressure leads for $Pr_{0.75}Na_{0.25}MnO_3$ to a suppression of the charge ordered insulating pseudo-CE-type AFM state and the appearance of the A-type AFM state without charge ordering. Unlike the case for $Pr_{0.8}Na_{0.2}MnO_3$, no formation of FM regions under high pressure in $Pr_{0.75}Na_{0.25}MnO_3$ was observed. The unexpected result is the out-of-plane orientation of manganese magnetic moments in the A-type AFM phase, which is at variance with the $d(x^2-y^2)$ orbital polarization. This observation suggests an exchange coupling between the A-type and pseudo-CE-type AFM regions of presumably nanoscopic thickness.

A possible reason for the stabilization of the A-type AFM phase is the compression anisotropy which leads to the apical contraction of MnO_6 octahedra under high pressure and creates favourable conditions for the appearance of the $d(x^2 - y^2)$ orbital polarization, a prerequisite for the A-type AFM order. With the stabilization of the A-type regions, the apical contraction becomes more pronounced but the crystallographic twinning and the presence of the residual pseudo-CE phase keep the average structure pseudo-cubic. Similarly to the case for structurally related manganites with similar doping, it is assumed that the onset of the A-type AFM state in $Pr_{0.75}Na_{0.25}MnO_3$ is accompanied with an insulator–metal transition. It is expected that the macroscopic transport will be severely influenced by grain and magnetic domain boundaries.

Acknowledgments

The authors thank W G Marshall and D J Francis for their help with ISIS experiments. The allocation of beam time and financial support from the ISIS and LLB facilities and the Russian Foundation for Basic Research grant 03-02-16879 are gratefully acknowledged.

References

[1] Dagotto E, Hotta T and Moreo A 2001 *Phys. Rep.* **344** 1
[2] Zener C 1951 *Phys. Rev.* **82** 403
[3] Anderson P W and Hasegawa H 1955 *Phys. Rev.* **100** 675
[4] De Gennes P-G 1960 *Phys. Rev.* **118** 141
[5] Maezono R, Ishihara I and Nagaosa N 1998 *Phys. Rev.* B **58** 11583
[6] Radaelli P G, Cox D E, Marezio M and Cheong S-W 1997 *Phys. Rev.* B **55** 3015
[7] Jirák Z, Krupićka S, Simsa Z, Dlouha M and Vratislav S 1985 *J. Magn. Magn. Mater.* **53** 153
[8] Millange F, De Brion S and Chouteau G 2000 *Phys. Rev.* B **62** 5619
[9] Kawano H, Kajimoto R, Yoshizawa H, Tomioka Y, Kuwahara H and Tokura Y 1997 *Phys. Rev. Lett.* **78** 4253
[10] Cox D E, Radaelli P G, Marezio M and Cheong S-W 1998 *Phys. Rev.* B **57** 3305
[11] Tomioka Y, Asamitsu A, Kuwahara H, Moritomo Y and Tokura Y 1996 *Phys. Rev.* B **53** R1689
[12] Jirák Z, Hejtmánek J, Kniźek K, Pollert E, Dlouhá M, Vratislav S, Kuźel R and Hervieu M 2002 *J. Magn. Magn. Mater.* **250** 275
[13] Miyano K, Tanaka T, Tomioka Y and Tokura Y 1997 *Phys. Rev. Lett.* **78** 4257
[14] Satoh T, Kikuchi Y, Miyano K, Pollert E, Hejtmánek J and Jirák Z 2002 *Phys. Rev.* B **65** 125103
[15] Moritomo Y, Kuwahara H, Tomioka Y and Tokura Y 1997 *Phys. Rev.* B **55** 7549
[16] Kozlenko D P, Voronin V I, Glazkov V P, Medvedeva I V and Savenko B N 2004 *Phys. Solid State* **46** 484
[17] Cui C, Tyson T A and Chen Z 2003 *Phys. Rev.* B **68** 214417
[18] Kozlenko D P, Glazkov V P, Jirák Z and Savenko B N 2003 *J. Magn. Magn. Mater.* **267** 120
[19] Besson J M, Nelmes R J, Hamel G, Loveday J S, Weill G and Hull S 1992 *Physica* B **180/181** 907
[20] Marshall W G and Francis D J 2002 *J. Appl. Crystallogr.* **135** 122
[21] Decker D L 1971 *J. Appl. Phys.* **42** 3239
[22] Von Dreele R B and Larson A C 1986 *Los Alamos National Laboratory Report* No LAUR 86 748
[23] Goncharenko I N, Glazkov V P, Irodova A V, Lavrova O A and Somenkov V A 1992 *J. Alloys Compounds* **179** 253
[24] Goncharenko I N, Mirebeau I, Molina P and Boni P 1997 *Physica* B **234–236** 1047
[25] Rodriguez-Carvajal J 1993 *Physica* B **192** 55
[26] Birch F J 1986 *J. Geophys. Res.* **91** 4949
[27] Meneghini C, Levy D, Mobilio S, Ortolani M, Nuñez-Reguero M, Kumar A and Sarma D D 2001 *Phys. Rev.* B **65** 012111
[28] Radaelli P G, Iannone G, Marezio M, Hwang H Y, Cheong S-W, Jorgensen J D and Argyriou D N 1997 *Phys. Rev.* B **56** 8265
[29] Kajimoto R, Yoshizawa Y, Kawano H, Tokura Y, Ohoyama K and Ohashi M 1999 *Phys. Rev.* B **60** 9506
[30] Hejtmánek J, Pollert E, Jirák Z, Sedmidubský D, Strejc A, Maignan A, Martin Ch, Hardy V, Kužel R and Tomioka Y 2002 *Phys. Rev.* B **66** 014426
[31] Damay F, Martin C, Hervieu M, Maignan A, Raveau B, André G and Boureé F 1998 *J. Magn. Magn. Mater.* **184** 71
[32] Konishi Y *et al* 1999 *J. Phys. Soc. Japan* **68** 3790
[33] Fang Z, Solovyev I V and Terakura K 2000 *Phys. Rev. Lett.* **84** 3169
[34] Chmaissem O, Dabrowski B, Kolesnik S, Mais J, Jorgensen J D and Short S 2003 *Phys. Rev.* B **67** 094431